EURASIAN JOURNAL OF MATHEMATICAL AND COMPUTER APPLICATIONS
ISSN 2306–6172
Volume 13, Issue 4 (2025) 31 – 40

ON THE REFRACTIVE INDEX RESTORATION BASED ON FOUR-ANGLE HILBERT TOMOGRAPHY DATA

Arbuzov E.V., Zolotukhina O.S. [1]

Abstract The paper considers the inverse problem of determining the refractive index of optical media using four-angle Hilbert visualization of phase disturbances. The phase functions for each projection (Radon data) are reconstructed using the Gauss-Newton iterative algorithm. The refractive index is determined using the Gerchberg–Papoulis algorithm based on a discrete analog of the central slice theorem for the four-angle case. The results of numerical modeling are presented.

Keywords: Hilbert optics, phase problem, low-angle tomography.

AMS Mathematics Subject Classification: 65R32.

DOI: 10.32523/2306-6172-2025-13-4-31-40

1 Introduction

The paper considers the problem of reconstructing the function $u(x, y, z)$ in a cylindrical domain $\{x^2 + z^2 \leqslant 1,\ y_1 \leqslant y \leqslant y_2\}$ from known values

$$\mathscr{H}[\varphi_k](x,y) = \left|\frac{1}{\pi}\int\limits_{\mathbb{R}} \frac{e^{i\varphi_k(\xi,y)}}{x-\xi}\,d\xi\right|^2 = \left(\frac{1}{\pi}\int\limits_{\mathbb{R}} \frac{\cos\varphi_k(\xi,y)}{x-\xi}\,d\xi\right)^2 + \left(\frac{1}{\pi}\int\limits_{\mathbb{R}} \frac{\sin\varphi_k(\xi,y)}{x-\xi}\,d\xi\right)^2$$
$$= (\mathscr{H}_{cos}[\varphi_k](x,y))^2 + (\mathscr{H}_{sin}[\varphi_k](x,y))^2. \tag{1}$$

Functions $\varphi_k(x_k, y)$ in each layer $y \in [y_1, y_2]$ are related to the unknown function $u(x, y, z)$ via Radon integrals

$$\varphi_k(x_k, y) = \int\limits_{\mathbf{r}\cdot\mathbf{e}_\mathbf{k}^\perp = x_k} u(x, y, z)dl, \tag{2}$$

here $\mathbf{r} = (z, x)$, $\mathbf{e_k} = (\cos\theta_k, \sin\theta_k)$, in four directions $\theta_k = \frac{\pi}{4}k$, $k = 0, \ldots, 3$.

This problem arises when using the methods of Hilbert optics to reconstruct the parameters of complex media.

If the phase filter $H(\omega_x, \omega_y)$ is placed in the Fourier plane of the shadow device, then the function recorded in the experiment (the object image) is set using the direct and inverse Fourier transform by the following expression

$$I(x,y) = \left|F^{-1}[H(\omega_x,\omega_y)\cdot\hat{s}(\omega_x,\omega_y)](x,y)\right|^2 = \left|F^{-1}[H] * s(x,y)\right|^2, \tag{3}$$

where $s(x, y) = a(x, y)e^{i\varphi(x,y)}$ is a signal containing information about the object under study.

Using linear filtering (3) allows visualizing phase distortions, since only the signal intensity $I_s = |s|^2$ is recorded in the optical radiation range, and phase information is lost. Hilbert optics allows solving the phase problem using the visualization method and is a contactless (non-destructive) method for studying and monitoring the parameters of optical inhomogeneities.

[1] Corresponding Author.

Optical visualization methods are usually divided into two large classes: the interferometric and the shadow ones. Interferometric methods are quantitative, since they are based on measuring the phase difference.

The shadow methods are characterized by the following:

– the inhomogeneity is visualized by introducing a diaphragm, which leads to a change in the phase or amplitude of a part of the light beam, causing redistribution of brightness in the image plane;

– the change in brightness is considered in the plane conjugate with the plane of inhomogeneity.

For a long time, the shadow methods, being effective in diagnosing optical inhomogeneities, allowed obtaining only qualitative information about the object under study. The work [1] of 1966, is one of the first publications, which noted the usefulness of the Hilbert transform in optical Fourier spectroscopy. Later, in 2003 and 2007, monographs [2], [3] were published, in which the methods of Hilbert optics are presented in the context of visualizing and measuring the fields of phase optical density. As a result, the theory of shadow methods was presented in the form of a compact mathematical apparatus.

Objects that change only the phase of the passing light wave are called optical inhomogeneities or phase objects. In the case of scanning with a plane-parallel wave, the field immediately behind the optical inhomogeneity can be described by function $s(x, y) = e^{i\varphi(x,y)}$, with the phase function $\varphi(x, y)$ carrying information about the properties of the object.

The use of a linear light source in a shadow device in combination with a quadrant phase Hilbert filter $H(\omega_x, \omega_y) = \operatorname{sgn}(\omega_x)\operatorname{sgn}(\omega_y)$, in each section y of the phase object provides one-dimensional Hilbert transform of the optical field $s(x, y)$ with respect to the variable x:

$$\tilde{s}(x, y) = \frac{1}{\pi} \int\limits_{-\infty}^{\infty} \frac{s(\xi, y)}{x - \xi}\, d\xi.$$

At that, the initial data for further processing is the intensity of the recorded signal (the brightness of the image recorded by a photo or video camera) $I[\varphi](x, y) = |\tilde{s}(x, y)|^2$, i.e. expression (1).

Thus, the inverse problem of Hilbert optics consists in reconstructing the phase function $\varphi(x, y)$ from the brightness values $I[\varphi](x, y)$ of the hilbertogram, which is recorded in the experiment. In [4], to calculate the phase function from Hilbert diagnostics data, it was proposed to use optimization methods, and this allows determining the numerical values of the phase optical density fields.

If the phase object is illuminated by a plane wave with a wavelength λ propagating along the z axis, then the phase function $\varphi(x, y)$ is related to the refractive index $n(x, y, z)$ of the medium under study by the Radon integral

$$\varphi(x, y) = \frac{2\pi}{\lambda} \int_{z'}^{z''} (n(x, y, z) - n_0) dz,$$

where n_0 is the refractive index of the surrounding medium, and z' and z'' are the points of the beam input and output relative to the local structure of the medium under study, i.e. by expression (2).

In the case of plane problems, the refractive index of the medium under study is reconstructed in an elementary manner. For axisymmetric structures, data processing is performed using the Abel transform [5], [6]. When solving the problem of diagnosing complex structures, it is necessary to use tomographic methods. At that, for optical tomography, the main problems are the insufficient number of projections or the small angular range of object diagnostics [7].

The Gerchberg-Papoulis iterative algorithm [8], [9] is one of the common methods for solving the problem of reconstructing structures under study in low-angle tomography [10]. It is based on the use of a priori information about the object under study in the spatial plane and known information about the object in the frequency plane, which is obtained from Radon data using the central slice theorem.

This paper proposes a method for reconstructing the spatial distribution of the refractive index of a phase object using data obtained as a result of four-angle Hilbert tomographic probing, based on the sequential application of the Gauss-Newton and Gerchberg-Papoulis algorithms. The result of numerical modeling are presented.

The proposed reconstruction method can be used to study the structure of flows and transport processes in gaseous, liquid and reacting media. Visualization of phase optical density fields in the study of these physical phenomena is an urgent task [11]-[13].

2 Reconstruction of the phase function using hilbertograms

In [4], it is proposed to use the Gauss-Newton optimization method to determine the phase function from hilbertograms and subsequently restore the parameters of the medium. This method allows one to determine the vector $P = (P_0, ..., P_{K-1})$, which minimizes the objective function

$$f(P) = ||F(P)||^2 = \sum_{n=0}^{N-1} [a_n(P) - b_n]^2.$$

The method consists of performing successive approximations P^{j+1}:

$$P^{j+1} = P^j - \alpha \, [J^T(P^j) J(P^j)]^{-1} J^T(P^j) \, F(P^j),$$

where $J(P) = \left[\frac{\partial a_n(P)}{\partial P_\kappa}\right]_{n=0,\,\kappa=0}^{N-1,\,K-1}$ is the Jacobian matrix of the first-order derivatives of function $F(P)$, J^T is the transposed matrix, j is the iteration number, α is the coefficient used to regulate the optimization step. In [4], numerical examples of this method application are given for the cases when the phase functions are set by Bernstein polynomials.

The experimental hilbertogram does not have a polynomial dependence. At that, in each y cross-section, it is defined in the range $[-x_0, x_0]_y$, beyond which the phase function is equal to zero, and, most importantly, its values are known on a discrete set of points $x_n = -x_0 + nd$, where $d = 2x_0/N$: $I[\varphi](x_n, y) = I_n$, $(n = 0, ..., N-1)$.

Therefore, for each cross-section y, the objective function is defined by the expression

$$f(P) = \|F(P)\|^2 = \sum_{n=0}^{N-1} \left(I_n - I[\varphi_P](x_n, y)\right)^2, \tag{4}$$

where $\varphi_P = \varphi_P(x, y)$ is the function depending on parameters P, which models the sought-for function.

When selecting parameters P for the initial approximation, it is necessary to use the following properties of the Hilbert filtering operator [3]:

– *pseudo-differentiability*: the hilbertogram is zero at points x, where $\frac{\partial}{\partial x}\varphi(x, y) = 0$, and has a maximum brightness at the discontinuity points $\varphi(x, y)$ with respect to the variable x;

– *quasi-periodicity*: if $\varphi(x)$ has an extremum at point x, then when the phase changes by 2π : $\varphi(x + d) = \varphi(x) + 2\pi$, an additional extremum appears on the hilbertogram in some neighborhood of point $x + d$ (but not in it itself!). Also, to determine the boundaries of the region and the nature of the behavior of the phase function at extremum or inflection points, it is necessary to use a priori information about the object of study, based on the conditions of the experiment.

In the case of a discontinuous piecewise smooth phase function, the initial approximation is chosen to consist of several sections, modeled by a third-order Bernstein polynom (Bezier

curve). If $P_\xi^q = (P_{\xi,0}^q, ..., P_{\xi,3}^q)$, $P_\eta^q = (P_{\eta,0}^q, ..., P_{\eta,3}^q)$ $(q = 1, \dots, Q)$ are the components of the datum vertex vectors of the Bezier curve with number q, then the phase function on this section is set in parametric form

$$\begin{aligned}\xi(t, P_\xi^q) &= (1-t)^3 P_{\xi,0}^q + 3(1-t)^2\, t P_{\xi,1}^q + 3(1-t)\, t^2 P_{\xi,2}^q + t^3 P_{\xi,3}^q,\\ \eta(t, P_\eta^q) &= (1-t)^3 P_{\eta,0}^q + 3(1-t)^2\, t P_{\eta,1}^q + 3(1-t)\, t^2 P_{\eta,2}^q + t^3 P_{\eta,3}^q,\end{aligned} \tag{5}$$

for $t \in [0, 1]$. Then

$$\begin{aligned}I[\varphi_P](x,y) = \frac{1}{\pi^2}\left(\int_{x_1^0}^{x_1^1} \frac{\cos(\varphi_P^1(\xi,y))}{x-\xi} d\xi + \int_{x_2^0}^{x_2^1} \frac{\cos(\varphi_P^2(\xi,y))}{x-\xi} d\xi + ... + \int_{x_Q^0}^{x_Q^1} \frac{\cos(\varphi_P^Q(\xi,y))}{x-\xi} d\xi\right)^2\\ + \frac{1}{\pi^2}\left(\int_{x_1^0}^{x_1^1} \frac{\sin(\varphi_P^1(\xi,y))}{x-\xi} d\xi + \int_{x_2^0}^{x_2^1} \frac{\sin(\varphi_P^2(\xi,y))}{x-\xi} d\xi + ... + \int_{x_Q^0}^{x_Q^1} \frac{\sin(\varphi_P^Q(\xi,y))}{x-\xi} d\xi\right)^2,\end{aligned}$$

where x_q^0, x_q^1 are the coordinates along the x axis of the starting and ending points of the Bezier curve with number q. At that, $x_q^1 = x_{q+1}^0$ $(q = 1, ..., Q-1)$.

By virtue of expression (5), in each interval (x_q^0, x_q^1) the variable $\xi = \xi(t, P_\xi^q)$, therefore $d\xi = \xi_t'(t, P_\xi^q)dt$. Additionally denoting $\varphi_P(t, P_\eta^q, y) = \varphi_P^q(\xi(t, P_\xi^q), y) = \eta(t, P_\eta^q)$, the integral operator $I[\varphi_P]$ can be written as

$$\begin{aligned}I[\varphi_P](x,y) &= \frac{1}{\pi^2}\left(\int_0^1 \frac{\cos(\varphi_P(t, P_\eta^1, y))}{x - \xi(t, P_\xi^1)} \xi_t'(t, P_\xi^1) dt + \ldots + \int_0^1 \frac{\cos(\varphi_P(t, P_\eta^Q, y))}{x - \xi(t, P_\xi^Q)} \xi_t'(t, P_\xi^Q) dt\right)^2\\ &+ \frac{1}{\pi^2}\left(\int_0^1 \frac{\sin(\varphi_P(t, P_\eta^1, y))}{x - \xi(t, P_\xi^1)} \xi_t'(t, P_\xi^1) dt + \ldots + \int_0^1 \frac{\sin(\varphi_P(t, P_\eta^Q, y))}{x - \xi(t, P_\xi^Q)} \xi_t'(t, P_\xi^Q) dt\right)^2\\ &= \mathscr{H}_{cos}^2[\varphi_P](x,y) + \mathscr{H}_{sin}^2[\varphi_P](x,y).\end{aligned}$$

Thus, in the case of processing hilbertograms, the components of the objective function (4) in each cross-section y can be written in the form

$$F(P) = \begin{pmatrix} I_0 - H_0(P) \\ \vdots \\ I_{N-1} - H_{N-1}(P) \end{pmatrix}, \qquad H_n(P) = I[\varphi_P](x_n, y), \quad n = 0, ..., N-1.$$

By calculating the corresponding derivatives of functions $I[\varphi_P](x,y)$, the following statement is proved.

Proposition 2.1. *The Jacobian matrix for the objective function $F(P)$ is written as*

$$J = \begin{pmatrix} \frac{\partial H_0}{\partial P_{\xi,0}^1} & \cdots & \frac{\partial H_0}{\partial P_{\xi,3}^Q} & \frac{\partial H_0}{\partial P_{\eta,0}^1} & \cdots & \frac{\partial H_0}{\partial P_{\eta,3}^Q} \\ \vdots & \ddots & \vdots & \vdots & \ddots & \vdots \\ \frac{\partial H_{N-1}}{\partial P_{\xi,0}^1} & \cdots & \frac{\partial H_{N-1}}{\partial P_{\xi,3}^Q} & \frac{\partial H_{N-1}}{\partial P_{\eta,0}^1} & \cdots & \frac{\partial H_{N-1}}{\partial P_{\eta,3}^Q} \end{pmatrix},$$

where for $n = 0, \dots, N-1$, $l = 0, \dots, 3$

$$\begin{aligned}\frac{\partial H_n}{\partial P_{\xi,l}^q} &= 2\mathscr{H}_{cos}[\varphi_P](x_n,y) \int_0^1 \frac{\sin(\varphi_P(t, P_\eta^q, y))}{x_n - \xi(t, P_\xi^q)} (\varphi_P(t, P_\eta^q, y))_t' W_l(t)\, dt\\ &- 2\mathscr{H}_{sin}[\varphi_P](x_n,y) \int_0^1 \frac{\cos(\varphi_P(t, P_\eta^q, y))}{x_n - \xi(t, P_\xi^q)} (\varphi_P(t, P_\eta^q, y))_t' W_l(t)\, dt,\\ \frac{\partial H_n}{\partial P_{\eta,l}^q} &= -2\mathscr{H}_{cos}[\varphi_P](x_n,y) \int_0^1 \frac{\sin(\varphi_P(t, P_\eta^q, y))}{x_n - \xi(t, P_\xi^q)} \xi_t'(t, P_\xi^q) W_l(t)\, dt\\ &+ 2\mathscr{H}_{sin}[\varphi_P](x_n,y) \int_0^1 \frac{\cos(\varphi_P(t, P_\eta^q, y))}{x_n - \xi(t, P_\xi^q)} \xi_t'(t, P_\xi^q) W_l(t)\, dt,\end{aligned}$$

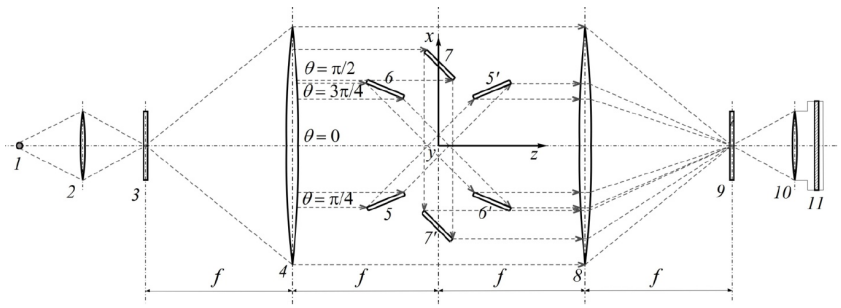

Figure 1: Schematic diagram of a four-angle Hilbert tomograph: radiation source 1, objective 2, slit diaphragm 3 placed in the front Fourier plane of objective 4, mirrors 5 and 5', 6 and 6', 7 and 7', forming probing beams oriented relative to the optical axis of the shadow device at angles $\theta_k = \pi k/4$, objective 8 with a quadrant phase Hilbert filter 9 in the frequency plane, video camera objective 10, video camera CCD matrix 11.

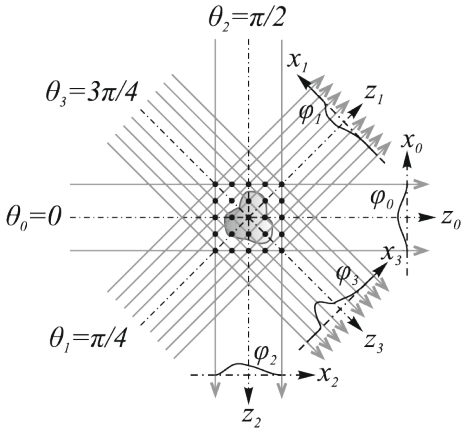

Figure 2: Obtaining values of phase functions φ_k (Radon data) in a Hilbert tomograph.

and $(W_0W_1, W_2, W_3)(t) = (1-t)^3,\ 3(1-t)^2t,\ 3(1-t)t^2,\ t^3)$.

3 Hilbert tomography

The developed optical complex (Fig.1) allows synchronous recording of visualized phase structures – hilbertograms $I[\varphi_k]$ – from four angles $\theta_k = \frac{\pi}{4}k$, $k = 0, ..., 3$, for several layers of the object, with one photo-video camera [14]. After reconstruction from hilbertograms for each projection of phase functions $\varphi_k(x_k, y)$, to determine the refractive index $u(x, y, z)$ in layer y from the obtained values, it is proposed to use the Gerchberg-Papoulis method, which is one of the most effective methods for reconstructing functions from their Radon data, especially in cases when the number of scanning directions is small or their angular range is limited [7]. The essence of the method is that a priori information about the sought-for function u and its known projections $\mathscr{R}u^k$ is used to create an initial approximation and subsequent correction in the coordinate and frequency spaces.

Many formulas for inverting the Radon problem are based on the central slice theorem, which states that the Fourier transform (one-dimensional) of projection $\mathscr{R}u^k$ is equal to the cross-section of the two-dimensional Fourier transform of function u. In the developed Hilbert tomograph, the mirrors and pixel structure of the photomatrices provide data acquisition in such a way that the projection values for all selected observation angles are determined at points that correspond to Radon integrals along the straight lines passing through the nodes of the sampling grid corresponding to the resolution of photomatrices (Fig. 2).

Therefore, the discrete analogue of the central slice theorem allows obtaining initial data

in the Fourier plane without preliminary interpolation. In a conventional tomograph, it would be necessary to perform interpolation or use different photomatrices for different directions.

If $u_{m,n}$, $m,n=0,...,N-1$ are discrete values with a sampling step $d=2/N$ of function $u(x,y,z)$ in cross-section y

$$u_{m,n}=u(x,z)\sum_{m=0}^{N-1}\sum_{n=0}^{N-1}\delta(x-nd,z-md),$$

and the scanning directions are determined by angles $\theta_k=\pi k/4$ $(k=0,...,3)$, then the Radon data are calculated using the formulas

$$\mathscr{R}u^0=(\sum_{m=0}^{N-1}u_{m,0}\,,\ldots,\sum_{m=0}^{N-1}u_{m,N-1}),\quad \mathscr{R}u^1=(\sum_{m+n=0}u_{m,n}\,,\ldots,\sum_{m+n=2N-2}u_{m,n},\,0),$$
$$\mathscr{R}u^2=(\sum_{n=0}^{N-1}u_{0,n}\,,\ldots,\sum_{n=0}^{N-1}u_{N-1,n}),\quad \mathscr{R}u^3=(0,\sum_{m-n=1-N}u_{m,n}\,,\ldots,\sum_{m-n=N-1}u_{m,n}).$$

The following statement is true (a discrete analogue of the central slice theorem for the four-angle tomography).

Proposition 3.1. *For the discrete Fourier transform of the values $u_{m,n}$*

$$\hat{u}_{m',n'}=\sum_{m=0}^{N-1}\sum_{n=0}^{N-1}u_{m,n}\,e^{-i\frac{2\pi}{N}(mm'+nn')},$$

and the discrete Fourier transform of the vector of projection $\mathscr{R}u^k$ (with dimension N_k)

$$\widehat{\mathscr{R}u^k}_{n'}=\sum_{n=0}^{N_k-1}\mathscr{R}u^k_n\,e^{-i\frac{2\pi}{N_k}nn'},$$

the following equalities are satisfied

$$\hat{u}_{0,n'}=\widehat{\mathscr{R}u^0}_{n'}\quad(n'=0,\ldots,N-1),\qquad \hat{u}_{m',m'}=\widehat{\mathscr{R}u^1}_{2m'}\qquad(m'=0,\ldots,N-1),$$
$$\hat{u}_{m',0}=\widehat{\mathscr{R}u^2}_{m'}\quad(m'=0,\ldots,N-1),\qquad \hat{u}_{m',N-m'}=\widehat{\mathscr{R}u^3}_{2m'}\quad(m'=1,\ldots,N-1).$$

Proof. Values $\hat{u}_{m',n'}$ for $m'=0$ are equal

$$\hat{u}_{0,n'}=\sum_{m=0}^{N-1}\sum_{n=0}^{N-1}u_{m,n}e^{-i\frac{2\pi}{N}nn'}=\sum_{n=0}^{N-1}\left(\sum_{m=0}^{N-1}u_{m,n}\right)e^{-i\frac{2\pi}{N}nn'}=\sum_{n=0}^{N-1}\mathscr{R}u^0_n e^{-i\frac{2\pi}{N}nn'}=\widehat{\mathscr{R}u^0}_{n'}.$$

Similarly, for $n'=0$

$$\hat{u}_{m',0}=\sum_{m=0}^{N-1}\sum_{n=0}^{N-1}u_{m,n}e^{-i\frac{2\pi}{N}mm'}=\sum_{m=0}^{N-1}\mathscr{R}u^2_m e^{-i\frac{2\pi}{N}mm'}=\widehat{\mathscr{R}u^2}_{m'}.$$

Then, for $m'=n'$

$$\hat{u}_{m',m'}=\sum_{m=0}^{N-1}\sum_{n=0}^{N-1}u_{m,n}e^{-i\frac{2\pi}{N}(m+n)m'}=\sum_{k=0}^{2N-2}\sum_{m+n=k}u_{m,n}e^{-i\frac{2\pi}{N}km'}=\sum_{k=0}^{2N-2}\mathscr{R}u^1_k e^{-i\frac{2\pi}{N}km'}.$$

Since $\mathscr{R}u^1_k=0$ for $k=2N-1$, then

$$\hat{u}_{m',m'}=\sum_{k=0}^{2N-1}\mathscr{R}u^1_k e^{-i\frac{2\pi}{N}km'}=\sum_{k=0}^{2N-1}\mathscr{R}u^1_k e^{-i\frac{2\pi}{2N}k\,2m'}=\widehat{\mathscr{R}u^1}_{2m'}.$$

In the case, where $n'=N-m'$ and $m'=1,\ldots,N-1$

$$\begin{aligned}\hat{u}_{m',N-m'} &= \sum_{m=0}^{N-1}\sum_{n=0}^{N-1} u_{m,n}e^{-i\frac{2\pi}{N}(mm'+n(N-m'))} = \sum_{m=0}^{N-1}\sum_{n=0}^{N-1} u_{m,n}e^{-i\frac{2\pi}{N}(m-n)m'} \\ &= \sum_{k=-N+1}^{N-1}\sum_{m-n=k} u_{m,n}e^{-i\frac{2\pi}{N}km'} = \sum_{k'=1}^{2N-1}\sum_{m-n=k'-N} u_{m,n}e^{-i\frac{2\pi}{N}k'm'} \\ &= \sum_{k'=1}^{2N-1} \mathscr{R}u^3_{k'}e^{-i\frac{2\pi}{N}k'm'} = \sum_{k'=0}^{2N-1} \mathscr{R}u^3_{k'}e^{-i\frac{2\pi}{2N}k'\,2m'} = \widehat{\mathscr{R}u^3}_{2m'},\end{aligned}$$

because $\mathscr{R}u^3_0 = 0$. □

Remark 1. *A zero element is added to the Radon data $\mathscr{R}u^1, \mathscr{R}u^3$ to make the dimension of the vector $2N$.*

Remark 2. *The number of elements in the Radon data is different: the dimension of projections $\mathscr{R}u^0, \mathscr{R}u^2$ is N. The projections $\mathscr{R}u^1, \mathscr{R}u^3$ contain $2N$ elements, whose values are taken at points $x_n = \frac{\sqrt{2}}{2}d\,n$. Therefore, to apply the formulas of Proposition 3.1, the data must be consistent. In the Hilbert tomograph, the recorded data are already consistent due to the choice of the geometry of the scanning directions, the use of mirrors and the pixel structure of the photo matrices!*

In this work, when applying the Gerchberg-Papoulis method, the non-negativity and finiteness of the sought-for function are used as a priori information:

$$u(x,y,z) \geq 0; \quad u(x,y,z) = 0, \quad x^2 + z^2 \geq 1.$$

These properties define the A_u operator acting in the spatial plane.

In the Fourier plane, the values of function $\hat{u}(\omega)$ on set M are known from the Radon data: in the directions along the vectors $\mathbf{e}^{\perp}_{\mathbf{k}}$, $\mathbf{e}_{\mathbf{k}} = (\cos\theta_k, \sin\theta_k)$. Thus, if χ_M is the characteristic function of set M, then the following values are known

$$U_M(\omega) = \chi_M(\omega)\hat{u}(\omega).$$

To reconstruct the refractive index function u, the following operations are performed:

1. Using the known Radon data $\mathscr{R}u^k$, the one-dimensional Fourier transforms are calculated. According to Proposition 3.1, function U_M is determined, equal to the values of the two-dimensional Fourier transform of the sought values of function u in the directions corresponding to the projection angles, and equal to zero at the remaining points of the Fourier plane.
2. The initial approximation u_0 is determined. The inverse two-dimensional Fourier transform of U_M is calculated and operator A_u is applied: a priori information about the non-negativity of function u and the finitness of the domain of its definition is entered.
3. The two-dimensional Fourier transform of the initial approximation is performed. Its values in the directions corresponding to the projection angles are replaced by the U_M values calculated in step 1.
4. The inverse two-dimensional Fourier transform of the values obtained in the previous step is performed, and operator A_u is applied to the result.
5. The criterion for the end of the iterative process is checked: the smallness of the value $\Delta^2_{j+1} = \frac{\sum_{m=0}^{N-1}\sum_{n=0}^{N-1}(u^{j+1}_{m,n} - u^j_{m,n})^2}{\sum_{m=0}^{N-1}\sum_{n=0}^{N-1}(u^j_{m,n})^2}$.

As a result, the reconstruction algorithm can be represented as

$$u^0 = A_u F^{-1}[U_M], \quad u^{j+1} = A_u F^{-1}[U_M + (1-\chi_M)\hat{u^j}].$$

The Gerchberg-Papoulis algorithm can be represented as iterative transitions from object evaluation in the spectral plane to its evaluation in the spatial plain, with the introduction of a priori information about the values of the function and its spectrum in each of domains during their execution. These transitions are carried out using the discrete Fourier transform algorithm. In this case, the quality of restoration will depend on the properties of function u itself and its Fourier transform $\hat{u}$. Examples of restoration of various functions by four projections are given in [14].

4 Numerical modeling

In this section, a numerical example is given to illustrate the operation of the proposed reconstruction algorithm. The refractive index is modeled by the function

$$u(x,z) = \sum_{j=1}^{3} a_j \, e^{-((x-x'_j)^2+(z-z'_j)^2)/s_j^2}.$$

To calculate hilbertograms from phase functions defined on a discrete set of points, the Hilbert transform is represented through the imaginary part of the analytical signal. When approximating the analytic signal, the Fourier transform of the input sequence is calculated, the Fourier coefficients that correspond to negative frequencies are replaced by zeros, and the inverse Fourier transform is calculated.

The phase function distributions obtained in each projection and the corresponding hilbertograms are shown in Fig. 3. Initial approximations by Bezier curves were constructed taking into account data on the boundaries of the region, the position and number of extremum points that determine the sections of function monotonicity and limit the range of its change in each section.

As a result of applying the Gauss–Newton optimization, the values of phase function with the following parameters were obtained for each tomographic projection:

– number of iterations $j_0 = 103$, $j_1 = 93$, $j_2 = 84$, $j_3 = 87$;
– rms error $\Delta = \left(\frac{1}{N}\sum\limits_{n=0}^{N-1}(I_n - H_n(P))^2\right)^{1/2}$;
– $\Delta_0 = 0,03$, $\Delta_1 = 0,02$, $\Delta_2 = 0,02$, $\Delta_3 = 0,01$;
– maximum deviation $c_0 = 0,3$, $c_1 = 0,26$, $c_2 = 0,29$, $c_3 = 0,22$.

Using the obtained values, the Gerchberg–Papoulis method was used to reconstruct function $u(x,z)$. The result of reconstructing the test function is shown in Fig. 4. The reconstruction of this object was performed using $j = 250$ iterations and rms reconstruction error $\Delta_j = 13.35\%$. The result of applying the back projection method with filtering to the values of $\mathscr{R}u^k$ is shown for comparison.

5 Summary and discussion

A method for reconstructing the spatial distribution of the refractive index of the object under study using data obtained during four-angle Hilbert tomographic probing was developed in the current research. The structure of the phase components, which is a function of the refractive index, for each projection (Radon data) is reconstructed using the iterative Gauss–Newton algorithm by minimizing the root mean square error between the experimental and model hilbertograms. Further, the initial value of the refractive index is determined using the Gerchberg–Papoulis algorithm, based on a discrete analogue of the central slice theorem in the four-angle case. The proposed method will be used to process data obtained during the experimental studies.

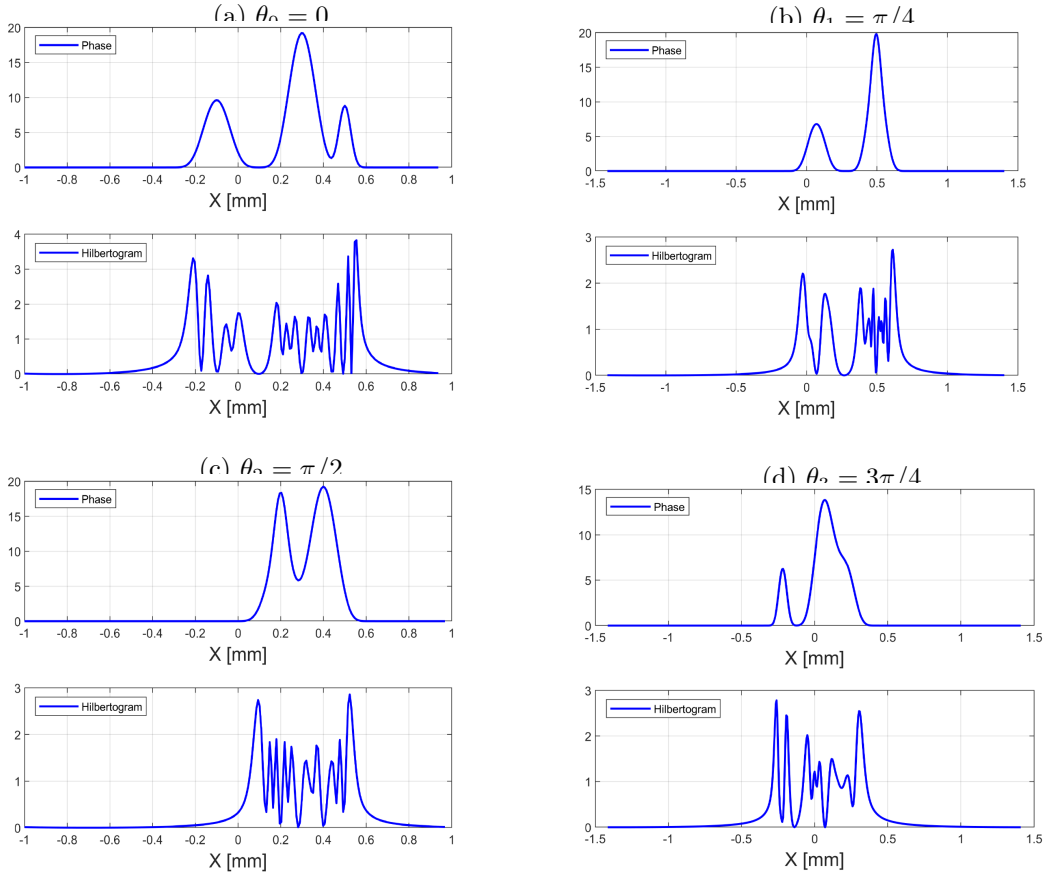

Figure 3: Distributions of the phase function obtained in each projection and the corresponding hilbertograms.

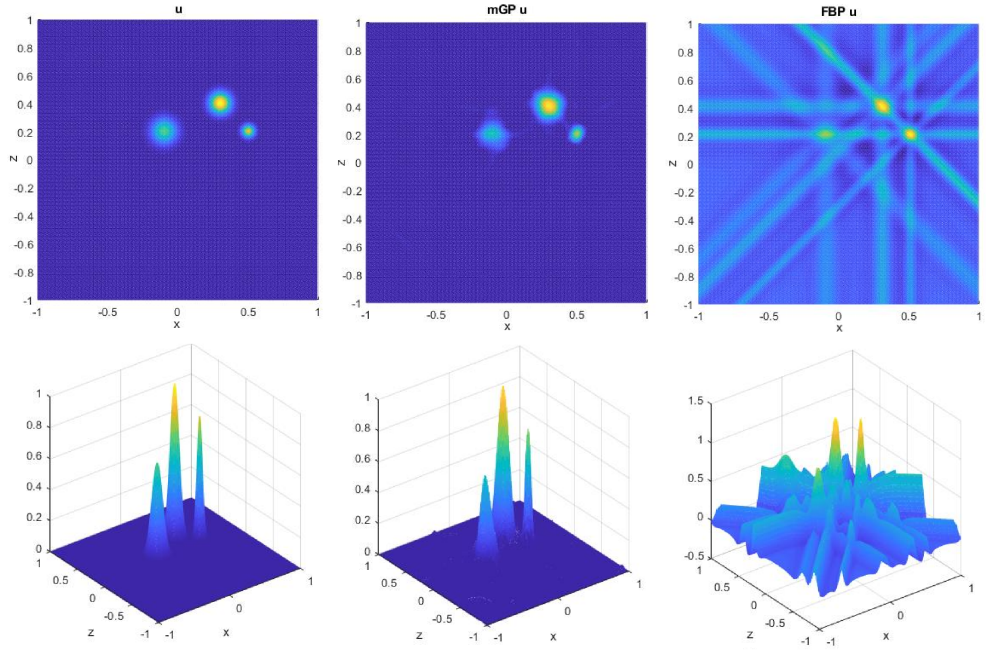

Figure 4: Initial function $u(x, z)$ and the result of reconstruction by the Gerchberg-Papoulis method (mGPu) and the method of back projection with filtering (FBP u).

Acknowledgement

The work of the first author was carried out within the framework of the state assignment of Sobolev Institute of Mathematics SB RAS (No. FWNF-2022-0009), and the work of the second author was carried out within the framework of the state assignment of Kutateladze Institute of Thermophysics SB RAS (No. 121031800217-8).

References

[1] H. Sakai, G. Vanasse, *Hilbert transform in Fourier spectroscopy*. Journal of the Optical Society of America, 56.1 (1966), 131-132. DOI: 10.1364/JOSA.56.000131.

[2] Yu.N. Dubnishchev, V.A. Arbuzov, P.P. Belousov, P.Ya. Belousov, *Optical Methods of Flow Investigation* [in Russian]. Sib. Univ. Publ., Novosibirsk, 2003.

[3] V.A. Arbuzov, Yu.N. Dubnishchev, *Methods of Hilbert-Optics in Measuring Technologies* [in Russian]. NSTU Publ., Novosibirsk, 2007.

[4] E.V. Arbuzov, O.S. Zolotukhina, *Gauss-Newton method application in the problem of phase function reconstructing from hilbertograms*. Eurasian Journal of Mathematical and Computer Applications, 11.4 (2023), 4–13. DOI: 10.32523/2306-6172-2023-11-4-4-13.

[5] Z.N. Ashrafi, M. Ashjaee, M.H. Askari, *Two-dimensional temperature field measurement of a premixed methane/air flame using Mach-Zehnder interferometry*. Optics Communications, 341 (2015), 55-63. DOI: 10.1016/j.optcom.2014.12.004.

[6] S.A. Coronel, J. Melguizo-Gavilanes, S. Jones, J.E. Shepherd, *Temperature field measurements of thermal boundary layer and wake of moving hot spheres using interferometry*. Experimental Thermal and Fluid Science, 90 (2018), 76-83. DOI: 10.1016/j.expthermflusci.2017.08.031.

[7] G.G. Levin, G.N. Vishnyakov, *Optical Tomography* [in Russian]. Radio i Svyaz, Moscow, 1989.

[8] R.W. Gerchberg, *Super-resolution through error energy reduction*. Opt. Acta, 21 (1974), 709-720. DOI: 10.1080/713818946.

[9] A.A. Papoulis, *New algorithm in spectral analysis and band-limited extrapolation*. IEEE Transactions on Circuits and Systems, 22 (1975), 735-742. DOI: 10.1109/TCS.1975.1084118.

[10] D. Kazantsev, V. Pickalov, *New iterative reconstruction methods for fan-beam tomography*. Inverse Problems in Science and Engineering, (2017), 1-19. DOI: 10.1080/17415977.2017.1340946.

[11] J. Feng, K. Okamoto, D. Tsuru, H. Madarame, M. Fumizawa, *Visualization of 3D gas density distribution using optical tomography*. Chemical Engineering Journal, 86 (2002), 243-250. DOI: 10.1016/S1385-8947(01)00185-1.

[12] J. Cao, K. Yang, X. Fang, L. Gou, Y. Li, Q. Cheng, *Holographic tomography of dynamic three-dimensional acoustic vortex beam in liquid*. Appl. Phys. Lett., 119.4 (2021), 143501. DOI: 10.1063/5.0062529.

[13] V. Rastogi, S. Agarwal, V. Kumar, C. Shakher, *Holographic optical element based digital holographic interferometer for the study of macro flames, micro flames and their temperature instability*. Optics and Lasers in Engineering, 122 (2019), 29-36. DOI: 10.1016/j.optlaseng.2019.05.021.

[14] E.V. Arbuzov, V.A. Arbuzov, Yu.N. Dubnishchev, O.S. Zolotukhina, M.M. Lapikov, V.V. Lukashov, *Possibility of using the Gerchberg–Papoulis method in the problem of phase structure reconstructing from low-angle hilbertograms*. Scientific Visualization, 16.1 (2024), 19-28. DOI: 10.26583/sv.16.1.02.

Eduard Arbuzov,
Sobolev Institute of Mathematics SB RAS,
Koptyug av. 4, 630090 Novosibirsk, Russia,
Email: arbuzov@math.nsc.ru

Olga Zolotukhina,
Kutateladze Institute of Thermophysics SB RAS,
Lavrentiev av. 1, 630090 Novosibirsk, Russia,
Email: zolotukhina@itp.nsc.ru.

Received 11.11.2024, Accepted 25.04.2025, Available online 31.12.2025.